Off-road tire modeling and the multi-pass effect for vehicle dynamics simulation

C. Senatore[a,1,*], C. Sandu[b,1]

[a]*Department of Engineering Science and Mechanics, Virginia Tech, Blacksburg, VA 24061, USA.*
[b]*Department of Mechanical Engineering, Virginia Tech, Blacksburg, VA 24061, USA.*

Abstract

Off-road operations are critical in many fields and the complexity of the tire-terrain interaction deeply affects the vehicle performance. Soft soil can drastically reduce the traction performance of tires up to the point of making the motion impossible. In this paper, a semi-empirical off-road tire model is discussed. The efforts of several researchers are brought together into a single model able to predict the main features of a tire operating in off-road scenarios by computing drawbar pull, driving torque, lateral force, slip-sinkage phenomenon and the multi-pass behavior. The approach presented in this paper is principally based on the approach proposed by Wong, Reece, Chan, and Sandu and it is extended in order to catch into a single model the fundamental features of a tire running on soft soil. A thorough discussion of the methodology is conducted in order to highlight strengths and weakness of different implementations. The study considers rigid wheels and flexible tires and analyzes the longitudinal and the lateral dynamics. Being computationally inexpensive a semi-empirical model can be easily incorporated in vehicle dynamics simulations and real time applications. To the best knowl-

*Corresponding author
Email addresses: themast@vt.edu (C. Senatore), csandu@vt.edu (C. Sandu)

edge of the authors, current vehicle dynamics codes poorly account for off-road operations where the tire-terrain interaction plays a crucial role in the prediction of the vehicle performance. In this paper two soils are considered: a loose sandy terrain and a firmer loam. The results show that the model realistically predicts the longitudinal and lateral forces providing at the same time good estimates of the slip-sinkage behavior and tire parameters sensitivity: this aspect is essential in order to realistically estimate the energy efficiency.
Keywords: off-road tire dynamics, slip sinkage, multi pass, lateral force, traction, tire parameter influence

List of Symbols

b	penetrometer characteristic length
β, δ, ζ	coefficients needed to calculate deflected tire shape
c	soil cohesion
c_0, c_1, c_{0f}, c_{1f}	coefficients related to the angle where maximum stress occur
F_x	drawbar, longitudinal force
F_y, F_{ybd}, F_{ys}	lateral force, lateral force due to bulldozing, lateral force due to shear
γ_s	soil density
ϕ	angle of internal friction of the soil
j_x, j_y	longitudinal and lateral shear displacement
k_c'	cohesion related soils parameter
k_ϕ'	angle internal friction related soil parameter
k_x, k_y	shear deformation modulus in the longitudinal and lateral direction
k_1, k_2, k_3	multi-pass coefficients
l_p'	projected contact patch length
n	Bekker sinkage coefficient
n_0, n_1	Bekker slip-sinkage coefficient
N_γ, N_c, N_q	Terzaghi bearing capacity factors
q	surcharge load
R_{eff}, R_u, R_l	effective, undeformed, and rolling radius
σ_n	normal stress along the contact patch
s_d	slip ratio
θ_m	angular coordinate along the contact patch where the maximum stress is reached
θ_e, θ_b	entry and exit angle
τ	tangential stress along the contact patch
z	sinkage
w	tire width

1. Introduction

Vehicle operation on unpaved surfaces is a field of interest in military, agriculture, construction, exploration, recreation, and mining applications. The tire-soil interaction determines the mobility of the vehicle and then characterizes its dynamics.

Mathematical models able to predict and describe the deformable nature of both the tire and the terrain have been developed in the past decades [2, 11, 34, 20] but with the exception of the model proposed by Harnisch et al. [12] none of the available approaches condensates into a single model all the features of a tire operating on unprepared terrain. A tire model for off-road simulations has to be able to predict not only the traction and the torque but also the slip-sinkage and the multi-pass effects. Four approaches have been used by the researchers: experimental, empirical, semi-empirical, and finite element analysis; all of them having their own strengths and weaknesses.

Experimental testing consists of direct evaluation taken in the field. This method produces results that are valid only for the particular testing conditions which are intrinsically difficult to be evaluated. It is extremely difficult to measure and maintain the experimental parameters during testing. The real soil hardly behaves as a homogeneous material and its properties easily change with location and weather conditions [26, 25].

The empirical method was primarily developed by the US Army Waterways Experiment Station (WES) to asses vehicle mobility on a ”go/no go” basis. It is based on some measured indexes, such as the cone index [9]. The cone index is obtained using a cone penetrometer and the mobility index is determined by empirical expressions based on vehicle weight, contact area, size of grouser, power

of the engine, and type of transmission.

In the semi-empirical methods, the soil strength parameters are obtained experimentally, and traction performance is predicted using computational calculation in order to analyze the stress distribution. The motion resistance is calculated by integrating the horizontal component of soil pressure in the contact patch. The gross traction is calculated from the relationship between shear stress and slip displacement of the soil [5, 7, 6, 8, 3, 11, 16, 17, 37, 38] Although the stress distribution is calculated theoretically, the geometry of the deformed tire must be assumed.

Finally we have theoretical models that necessarily rely on finite element algorithms for solutions. Some researchers [23, 39, 19] also attempted to model the soil with discrete element (DE) and the tire with finite element (FE). In FE applications the soil is usually modeled as a visco-plastic/elasto-plastic/elastic-perfectly plastic material and the tire as a visco-elastic material. These models have the capability of a full three dimensional description but they require a large computational effort and are unsuitable for real-time simulations [30, 24, 29].

Semi-empirical methods are particularly attractive for vehicle dynamics simulations because they provide a good understanding and description of the physics underlying the problem and yet they are computationally effective for full scale analysis.

2. Tire Model and Assumptions

The model presented in this paper accounts for both rigid wheels and flexible tires. The rigid wheel can be considered a first approximation of a flexible tire. When the terrain stiffness is significantly lower than the total tire stiffness (the

carcass stiffness plus the inflation pressure), the flexible tire can be approximated as a rigid wheel, greatly simplifying the analysis. The study of rigid wheels is relevant as some vehicles are natively equipped with rigid wheels. This is the case of robots for extraterrestrial exploration [33, 1, 22] where rubber compounds cannot be used because of the severe environmental conditions (extreme temperature gradients and, possibly, unfavorable atmospheric chemical composition). The rigid wheel implementation is based on models developed by Wong and Reece [37] while the flexible tire implementation follows the approach proposed by Chan and Sandu [5, 7, 6]. The original formulations have been modified in several aspects in order to improve the model capabilities. These aspects will be clarified in the following sections where the model peculiarities will be explained.

2.1. Pressure-Sinkage Equation

The first step for a semi-empirical method is to estimate the stress distribution along the contact patch. Normal and shear stresses develop at the interface between a rotating tire and the soil surface. Normal stress is calculated from the pressure-sinkage equation originally introduced by Bekker and later modified by Reece (1):

$$p = (ck'_c + b\gamma_s k'_\phi)\left(\frac{z}{b}\right)^n, \tag{1}$$

where p is the pressure, z is the sinkage, c is the cohesion of the soil, k'_c and k'_ϕ are soil parameters related to the cohesion and the angle of shearing of the material, and b is a parameter related to the geometry of the penetrometer (the radius for circular plates or the smaller linear dimension for rectangular plates). Equation (1) is a modified version of the Bekker sinkage-pressure expression where the ratio

z/b is introduced for two reasons: to make the parameters k_c' and k_ϕ' dimensionless and provide a single equation that accounts for different plate shapes. The exponent n, is crucial because it defines the trend of the relationship.

2.1.1. Discussion on the Use of The Reece Equation for Tire Stress Distribution Estimation

In the terramechanics community it is widely accepted to use the Reece-Bekker equation to calculate the normal stress distribution along the contact patch of a tire. In order to have a better understanding of the limitations and features of this formulation some remarks are necessary. During the characterization of (1) the constants are obtained for a plate sinking perpendicularly to the terrain surface; the pressure acts along the z direction. For a sinking wheel, the stress calculated at any sinkage is considered to act along the radial direction of the wheel and not along the z direction. Another approximation is represented by the fact that the tire contact patch is thought as the penetrometer plate: the former one has a round shape while the latter has a flat contact surface. The Reece equation is obtained under uniaxial loading conditions while the rotating tire not only exerts a vertical load but it also applies shear during the penetration. It should be mentioned here that this formulation also assumes the terrain to be homogeneous and isotropic.

These approximations should be kept in mind in order to understand the great variability of experimental results.

2.2. Shear Stress

The calculation of the shear stress beneath the wheel is based upon an empirical expression first introduced by Janosi and Hanamoto [16] and widely used:

$$\tau_x(\theta) = \tau_{max}\left(1 - e^{\frac{-j_x}{k_x}}\right), \tag{2}$$

where τ_{max} is the limiting shear stress, j_x is the shear displacement of the terrain, and k_x is the shear deformation modulus which has to be estimated experimentally and it has a strong impact on the prediction of the shear stress.

The limiting shear stress τ_{max} can be related to the normal stress through the Mohr-Coulomb equation:

$$\tau_{max} = c + \sigma_n(\theta)\tan\phi, \tag{3}$$

where c is the cohesion as seen in (1) and ϕ is the angle of shear resistance. It should be mentioned that the terrain below a rolling tire is under a complex stress state which theoretically is not properly represented by the Mohr-Coulomb failure criterion as expressed by (3). The shear displacement j_x is calculated integrating the shear velocity of the terrain in contact with the wheel (assuming that the velocity of terrain particles at the interface matches the velocity of the tire):

$$j_x(\theta) = \int_{\theta_b}^{\theta_e} R_{eff}(\theta)[1 - (1 - s_d)\cos(\theta)]\, d\theta. \tag{4}$$

Notwithstanding the discussed approximations, equations (2),(3), (4) have shown to describe fairly well the shear distribution over a wide range of terrains [36].

2.3. Normal and Tangential Stress Distribution

The normal stress is calculated from (1) where the sinkage z is substituted by the following expression:

$$z = R_{eff}(\cos(\theta) - \cos(\theta_e)), \tag{5}$$

The angle θ is the central angle (i.e. the angle describing the angular position of the tire element starting counterclockwise from the bottom of the tire), θ_e is the entry angle (i.e. the angle at which the terrain enters in contact with the wheel), and R_{eff} is the effective radius which will be discussed later in section 2.4. Substituting (5) into (1) leads to a pressure distribution along the contact patch that starts from zero at the entry angle and monotonically increases. The maximum is reached at the point where the highest sinkage occurs; this point, for a rigid wheel, is necessarily located at the bottom of the wheel. This method has been adopted by Harnisch et al. [12] but it should be noted that experiments and the theory of plastic equilibrium [18, 34] show that the maximum of the pressure distribution occurs somewhere half-way between the entry and exit angles and is a function of the slip ratio; even though the sinkage increases monotonically from the entry angle to the bottom of the wheel, the stress distribution does not follow this trend (see Fig. 3). In order to reproduce a stress distribution similar to the one highlighted in the experiments, the normal stress is defined in this study as a piecewise function [37]. From the leading edge θ_e to the location of the maximum normal stress, θ_m, the stress is calculated using (6),

$$\sigma_{nf}(\theta) = (ck_1 + b\gamma_s k_2)\left(\frac{R_{eff}}{b}\right)^n (\cos(\theta) - \cos(\theta_e))^n, \tag{6}$$

while the normal stress that goes from the maximum stress point, θ_m, to the trailing edge, θ_b, can be evaluated with (7),

$$\sigma_{nr}(\theta) = (ck_1 + b\gamma_s k_2)\left(\frac{R_{eff}}{b}\right)^n \left(\cos\left(\theta_e - \left(\frac{\theta - \theta_r}{\theta_N - \theta_r}\right)(\theta_e - \theta_N)\right) - \cos(\theta_e)\right)^n. \tag{7}$$

In these equations the quantity b is defined as:

$$b = \min\left(l'_p, w\right), \tag{8}$$

where l'_p is the projected contact patch length and w is the tire width. This distinction is important because for some tire geometry the smaller dimension of the contact patch is the contact patch length and not the tire width.

With this implementation it is crucial to correctly estimate the value of θ_m. Chan and Sandu [5] proposed a method based on the Mohr-Coulomb failure criterion and the theory of plastic equilibrium: this approach is elegant but does not always lead to accurate results in terms of sinkage prediction [5, 31]. In this study, θ_m is thought to be a linear function of the slip ratio and the entry angle. This is an empirical estimation successfully implemented in other studies [37, 28, 21].

$$\theta_m = (c_0 + c_1|s_d|)\theta_e \tag{9}$$

where c_0 and c_1 are two constants. Since θ_m is usually half-way between the entry angle and exit angle, c_0 can be selected in the range of $[0.4, 0.5]$ and $c_1 \in [0.2, 0.4]$ [37]. Equation (9) guarantees that θ_m increases with the slip resulting in a better prediction of slip-sinkage behavior. It should be mentioned that Wong has suggested a different definition of θ_m for negative slip: however such definition creates discontinuity issues around zero slip and thus it was not considered here. Another method adopted to improve the calculation of slip-sinkage is to linearly relate the Bekker-Reece sinkage exponent n to the slip ratio [21].

$$n = n_0 + n_1|s_d|. \tag{10}$$

This is again an empirical approximation but it contains some physical insight. The exponent n is experimentally obtained for steady soil loading tests performed with a penetrometer. The response of the soil in contact with a rolling/slipping tire is presumably different. Equation (10) describes this phenomenon as suggested in

[21].

2.4. Rigid Wheel and Flexible Tire

A tire operating on deformable soil can be approximated as a rigid wheel if the pressure distribution along the contact patch does not exceed the inflated carcass stiffness. When this is verified the effective radius is a constant, and it equals the undeformed radius, $R_{eff} = R_u$. When the inflated carcass pressure is exceeded, the tire deforms and a different approach is needed. The problem becomes extremely complex because both the tire and the terrain are deformable. Chan and Sandu proposed to calculate the deflected shape of the tire through the following equation:

$$R_{eff} = \begin{cases} R_u - R_u\left(1 - \frac{1-\frac{\delta}{R_u}}{\cos(\theta)}\right) & \text{if } \theta_r < \theta \leq \theta_f \\ R_u - R_u\left(1 - \frac{1-\frac{\delta}{R_u}}{\cos(\theta_f)}\right) e^{-\beta\left(\sqrt{1+\zeta^2}+\zeta\right)(\theta-\theta_f)} & \text{if } \theta_f < \theta \leq \pi \\ R_u - R_u\left(1 - \frac{1-\frac{\delta}{R_u}}{\cos(2\pi+\theta_r)}\right) e^{\beta\left(\sqrt{1+\zeta^2}-\zeta\right)(\theta-(2\pi+\theta_r)} & \text{if } \pi < \theta \leq 2\pi+\theta_r \end{cases} \tag{11}$$

where ζ and β are two parameters related to the stiffness, damping, size, inflation pressure, angular velocity and construction of the tire and are obtained experimentally [5]. An example of a deformed tire is given in Figure 2. The tire has a flat shape between the angles θ_f and θ_r and a round shape (connected through a logarithm spiral) elsewhere.

The Harnisch et al. model [12] adopts the larger substitute circle to model the behavior of an elastic tire. The basic principle was suggested by Bekker but never carried out because of the complexity of the calculation. This approach consists in the substitution of a larger radius for the calculation of the contact patch: this

allows one to have a flatter contact region that mimics the shape of a deflected tire. This approach led to satisfactory results, but in this study the method proposed by Chan and Sandu is preferred because:

- it provides a more solid theoretical approach,
- the shape parameters can be calculated from physical characterization tests,
- it directly relates tires properties such as the inflation pressure and the carcass stiffness to the tire vertical deformation (a parameter easily obtainable from direct testing),
- the calculated shape matches the experimental results obtained by Freitag [10].

When the tire is driven on deformable soil, the flat section between θ_f and θ_r (first line of (11)) rotates counterclockwise [10, 18]. This phenomenon determines the amount of sinkage and it is a function of the slip, the vertical load and the inflation pressure. Assuming that the maximum deflection of the tire corresponds to the point where the maximum stress occurs, the rotation of the flat section can be set equal to the angle θ_m. Thus, for flexible implementation θ_m is calculated as follow:

$$\theta_m = \left(\frac{p_i F_z}{p_{i0} F_{z0}} c_{0f} + c_{1f} |s_d| \right) \theta_e \tag{12}$$

where p_{i0} is the nominal inflation pressure, F_{z0} is the load at which the tire carcass total stiffness is exceeded, and c_{0f} and c_{1f} are two empirical parameters similar to the ones introduced in (9) but now referred to flexible conditions. Equation 12 ensures that the predicted sinkage increases with vertical load and decreases with inflation pressure.

2.5. Drawbar Pull, Driving Torque, and Lateral Force

Once the normal and tangential stress distributions are known it is possible to calculate the drawbar pull and the driving torque. The balance of vertical forces needs to be calculated first: it ensures that the vertical force produced along the contact patch balances the vertical load of the vehicle, as given in (13).

$$W = w \int_{\theta_b}^{\theta_e} R_{eff}(\theta) \left(\sigma_n(\theta) \cos(\theta_{eff}) + \tau_x(\theta) \sin(\theta_{eff}) \right) d\theta, \qquad (13)$$

W is the weight force of the vehicle and the right hand side term represents the integrated stress along the contact patch acting in the vertical direction (i.e., the vertical force exerted by the tire). The angle θ_{eff} is the effective angle that the deformed tire shape creates with the vertical axis; for the rigid wheel model θ_{eff} is equal to θ. Equation (13) introduces two unknowns: the entry angle θ_e and the exit angle θ_b. The exit angle is smaller than the entry one because the wheel (rigid or flexible) is sinking into the ground and it is compacting the terrain while moving forward (see Fig. 1). Since no other analytical expressions can be derived, θ_b is estimated as follows (a distinction between the rigid wheel and flexible tire operational mode is required):

For rigid wheel implementation, the exit angle is assumed to be constant and small in magnitude. The wheel necessarily leaves the terrain flat and so the exit angle cannot physically be large (indeed, it is not equal to zero because of frictional phenomenon that displace the ground under the rotating wheel and because of the elastic response of the terrain). The value of the exit angle plays a important role in the determination of tractive performance. In fact, θ_b influences the size and location of the contact patch and can drastically change the model outcome.

For flexible tire implementation we propose to calculate the exit angle based

on the lowest point in contact with the terrain. After calculating the shape of the tire (11) and the counterclockwise rotation (i.e., θ_m calculated in (12)) it is assumed that the lowest point in the tire deformed configuration is the last point in contact with the terrain and θ_b is calculated accordingly; the entry angle θ_e is still determined by (13).

Drawbar pull (labeled as F_x) is calculated from the integration of the normal and shear stresses decomposed along the longitudinal direction.

$$F_x = w \int_{\theta_b}^{\theta_e} R_{eff}(\theta) \left(\tau_x(\theta) \cos(\theta_{eff}) - \sigma_n(\theta) \sin(\theta_{eff}) \right) d\theta. \tag{14}$$

It should be mentioned that this expression already includes soil compaction resistance given by the last term of the integral.

The driving torque is given by the following expression:

$$T = w \int_{\theta_b}^{\theta_e} R_{eff}^2(\theta) \tau_x(\theta) d\theta. \tag{15}$$

The lateral force F_y is generated by the lateral shear displacement j_y and by the bulldozing effect (due to the tire sinkage and soil surcharge, see Fig. 5). The component F_{ys} associated with the lateral shear is calculated similarly to (2), as given in (16).

$$F_{ys} = w \int_{\theta_b}^{\theta_e} \tau_y(\theta) d\theta = b \int_{\theta_b}^{\theta_e} (c + \sigma_n(\theta) \tan(\phi)) \left(1 - e^{\frac{-j_y}{k_y}} \right) d\theta. \tag{16}$$

The lateral force F_{ybd} associated with the bulldozing effect is calculated as a function of the sinkage, z, as presented in (17).

$$F_{ybd} = w \int_{\theta_b}^{\theta_e} (\gamma_s z N_\gamma + c N_c + q N_q) \cos(\delta_f) d\theta, \tag{17}$$

where N_γ, N_c, N_q are the Terzaghi's bearing capacity parameters; q is represents the surcharge load from accumulated bulldozed soil and δ_f is the angle between the normal to the surface of the side of the wheel and the direction of motion. Equation 17 is based on the Terzaghi bearing capacity equation [32] and the Hettiaratchi-Reece equation [13] for a wall moving into a mass of soil. It was adopted for the first time by Schwanghart [27], to model the pressure on the side-wall of a sinking tire. The total lateral force acting on the tire can be calculated through:

$$F_y = F_{ys} + F_{ybd}. \tag{18}$$

During combined slip operation the lateral and longitudinal shear stresses acting at the contact patch are limited by a failure envelope. The following criterion is adopted:

$$\left(\frac{\tau_x}{\tau_{xmax}}\right)^2 + \left(\frac{\tau_y}{\tau_{ymax}}\right)^2 \leq 1. \tag{19}$$

During cornering the soil undergoes complex loading state and the adoption of (19) represents only the first approximation as previously discussed for the definition of τ_{max}.

2.6. Multi-Pass Effect

Multi-pass effect has a strong impact on the evaluation of traction of off-road vehicles. Repetitive loading of deformable soils showed that during the unloading and reloading process the pressure-sinkage relation can be approximated with a straight line [34]. However, the modeling of repetitive loading introduced by

Wong cannot be directly implemented into the model because of the way the normal stress along the contact patch have been obtained (a piecewise function that does not strictly follow the monotonic trend of the sinkage). In this paper a different approach is taken. The most relevant study concerning the multiple pass of wheels on the same patch of terrain is the one performed by Holm [14]. The study showed that the terrain changes its properties after each pass and the variations are a function of the slip. If the first wheel is towed (zero torque pass) the terrain properties vary mildly, while the passage of a slipping tire produces a stronger effect on the soil. Holm's results are reproduced in figure 4 where the experimental results are fitted through the following equation:

$$\gamma_{sn} = \gamma_s \left[1 + \left(1 - e^{\frac{-s_0}{k_1}} \right) k_2 + k_3 n_p \right], \tag{20}$$

where k_1, k_2, k_3, are three fitting constants that can be derived from experiments while s_0 is the splip of the previous pass and n_p is the number of passes. The greatest variation occurs between the first and second pass: successive runs have less impact on the behaviour of the terrain. Terrain density increases after each pass and, considering the obtained results and related work from Bekker [3], also the cohesion of the material is considered to have increased. This phenomenon is incorporated into the model introducing a dependency of soil properties c, and k_x upon the number and type of passes through the following equations:

$$c_n = c \left[1 + \left(1 - e^{\frac{-s_0}{k_1}} \right) k_2 + k_3 n_p \right], \tag{21}$$

$$k_{xn} = k_x \left[1 - \left(1 - e^{\frac{-s_0}{k_1}} \right) k_2 - k_3 n_p \right]. \tag{22}$$

We speculate that c and k_x follow the same trend as in (20); thus, k_1, k_2, k_3 have the same value in (20),(21),(22).

2.7. Traction Efficiency

During off-road operations the energy efficiency of vehicle is deeply depending on the tires performance: the motion resistance at the tire-soil interface is dominantly influenced by the terrain compaction that results from sinkage. A measure of the efficiency can be obtained comparing the thrust power with the driving power:

$$\eta_t = \frac{F_x v_x}{T\omega} = \frac{F_x(1-s_d)R_l}{T}, \tag{23}$$

The efficiency depends upon the slip and the effective rolling radius R_l and it gives a measure of the capability to convert power delivered to the wheels into effective mobility. An exhaustive discussion on tractive efficiency is given by Zoz and Grisso [40]. Their analysis focuses on agricultural tires but it can be extended, without loss of generality, to off-road vehicles in general. Adopting the Brixius approach [4] they discuss the performance and efficiency of agricultural tractors. The outcomes are:

- Peak of tractive efficiency is reached in the 10-20% slip range.
- Larger tires provide better efficiency.
- Lower inflation pressure increases the tractive efficiency.
- Increased axle load has contrasting effects.

A tire model for vehicle simulation has to correctly predict the aforementioned results in order to provide realistic estimates of the energy consumption.

3. Results

The results are divided into three subsections: dry sand, moist loam and tractive efficiency. Dry sand is a non-cohesive and loose soil: on such terrain the inflated carcass pressure is never exceeded and the tire operates as a rigid wheel. Moist loam is a firmer soil which exhibits a steeper pressure-sinkage curve: on this terrain both the soil and the tire deforms.The aforementioned sections will discuss the longitudinal and lateral traction, the sinkage and the multi-pass effect. The last subsection will illustrate a comparison of the tractive efficiency under different operational parameters and soil conditions. Soil properties adopted in this research are extrapolated from [35] and summarized in Table 1. The correct estimation of these variables is crucial in order to obtain accurate results. Nominal tire properties are presented in Table 2 while the parameters introduced in the previous sections are summarized in Table 3.

3.1. Dry Sand - Rigid Wheel

3.1.1. Longitudinal Motion

On dry sand the tire operates as a rigid wheel. Figure 6 shows the trend of the drawbar pull and torque versus slip ratio at different vertical loads. The longitudinal force is much higher (in absolute value) for negative slip because of the sinkage phenomenon: terrain compaction force always acts against the direction of travel.

3.1.2. Lateral Motion and Combined Slip

Figure 7 shows the trend of lateral force versus slip angle α_c for various slip ratios and vertical loads. While tires rolling on hard surfaces (i.e., on-road) show a flat response for higher slip angle this does not happen on soft terrain: the lateral

force does not exhibit a maximum. This happens because the lateral force is due not only to the shear displacement at the contact patch but also to the bulldozing effect (see (18)). The term F_{ys} saturates for large slip angles but the term F_{ybd} monotonically increases because of the slip-sinkage phenomenon. Same results have been obtained by [27].

Figure 8 presents the combined slip F_y vs. F_x for various slip angles and vertical loads. The plot is biased towards negative values of drawbar pull because of the slip-sinkage behavior. Combined slip envelopes degenerate for larger slip angles: during off-road maneuvering the forces that the tire is able to exchange with the terrain are limited. For modest values of vertical loads (compared to the tire geometry) it is possible to obtain combined slip results for larger slip angles [15].

Combined slip plots are useful to understand the behavior of the tire during steering maneuvers. For instance, figure 8 predicts that for 5000N, positive drawbar is attainable only into a small range corresponding to high level of slip. This means that while steering drawbar is reduced and more slip is necessary to recover longitudinal thrust.

3.1.3. Multi-pass on Dry Sand

The multi-pass effect can radically change the performance of tires rolling into ruts created by other tires of the same or other vehicles. Figure 9 shows the variations of drawbar pull and sinkage for multiple passages predicted by the model. As mentioned previously the way the first pass is performed affects the terrain properties and the performance of the second pass. This has direct implications for multi-axle vehicles where only some of the axles are driven. The drawbar pull increases at the successive passages while the relative sinkage decreases because

of terrain compaction.

3.2. Moist Loam - Flexible Tire

3.2.1. Longitudinal Motion

On moist loam the tire operates in the flexible mode: plots presented in this section are similar, in nature, to plots presented for dry sand. Loam is a firmer soil, thus sinkage effect is reduced; this leads to improved drawbar pull capabilities. Figure 10 shows the trend of the drawbar pull and torque versus the slip ratio at different vertical loads.

Figure 11 presents the drawbar pull and the sinkage at various inflation pressure. Decreasing the inflation pressure provides a larger contact patch that helps improve the traction and at the same time reduces the sinkage.

3.2.2. Lateral Motion and Combined Slip

Figure 12 shows the trend of lateral force versus slip angle α_c for various slip ratios and vertical loads. The results are similar to the ones obtained with rigid wheels on dry sand; lateral force does not exhibit a maximum.

Figure 13 presents the combined slip F_y vs. F_x for various slip angles and vertical loads. Also, in this case, the flexible tires behave similarly to the rigid wheels.

3.2.3. Multi-pass on Moist Loam

Also when the tires behaves in a flexible way the multi-pass effect produces similar results. Successive passes increase the traction capability and decrease the relative sinkage, this is shown in Figure 14.

3.3. Traction Efficiency

Traction efficiency is presented in Figure 15. The efficiency increases for larger tires, lower inflation pressure and successive pass traveling on firmer soil (loam in this case). This happens because in these conditions the sinkage decreases leading to a reduced resistance compaction force. In on-road operations higher inflation pressure guarantees better fuel economy but this is not the case in off-road. Reduced inflation pressure not only improves the traction but it also reduces the sinkage and then it improves the efficiency as well (the hysteresis losses are negligible if compared with the terrain compaction resistance). The efficiency has a peak in the range of 10-20% slip but it should be remembered that it is not possible to impose the tires to work at an imposed slip ratio (the slip is indirectly controlled by the driver through the control of the desired vehicle speed). What can be done is to properly match the tires, the power-train ratio and the torque distribution in order to optimize the motion:this will be addressed in a future study.

4. Conclusions

In this paper, an enhanced off-road capable tire model has been proposed. The semi-empirical approach, well established in the terramechanics community, has been discussed and improved in order to combine, into a single model all the salient features that an off-road tire exhibits. The model is sensitive to tire geometry and consistently predicts the response to variable tire load and inflation pressure.

This study shows that it is licit to assume the exponent of Bekker equation n function of the slip. This ensures a more accurate estimate of the sinkage without deteriorating the prediction of the traction and torque. An adequate tuning of the

parameters introduced in (10), (9), (21), (20), (22) allows one to obtain from a single model consistent measures of drawbar pull, torque, lateral force, sinkage, multi-pass effect. These parameters can be identified from terrain and tire testing.

The methodology proposed is particularly suited for off-road vehicle dynamics simulations where it guarantees satisfactory accuracy and sensitivity to tire geometry [REF TER477].

Table 1: Undisturbed soil properties adapted from [35] simulations.

Soil	k_c'	k_{phi}'	n	c [Pa]	ϕ [deg]	k_x,k_y [m]	γ_s [N/m^3]
Dry Sand	34	49.68	0.70	1150	31.1	0.015	15,696
Moist Loam	24.45	96.34	0.97	3300	33.7	0.0076	15,196

Table 2: Nominal tire properties needed to calculate tire geometry. Parameters are referred to a Continental Contitrac SUV P265/70/R17 and have been experimentally calculated in [5].

R_u [m]	w [m]	p_i [kPa]	ζ	β	δ
0.4	0.265	240	0.0845	6.3579	0.0230

Table 3: Tire parameters for slip-sinkage and multi-pass calculation. c_0 and c_1 are taken from [37]. c_{0f} and c_{1f} are estimated by inspection. n_0 and n_1 are taken from [21]. k_1, k_2, and k_3 are extrapolated form [14] as explained in the text. All parameters are dimensionless.

c_0	c_1	c_{0f}	c_{1f}	n_0	n_1	k_1	k_2	k_3
0.4	0.2	0.2	0.05	0.8	0.6	0.1178	0.1672	0.0348

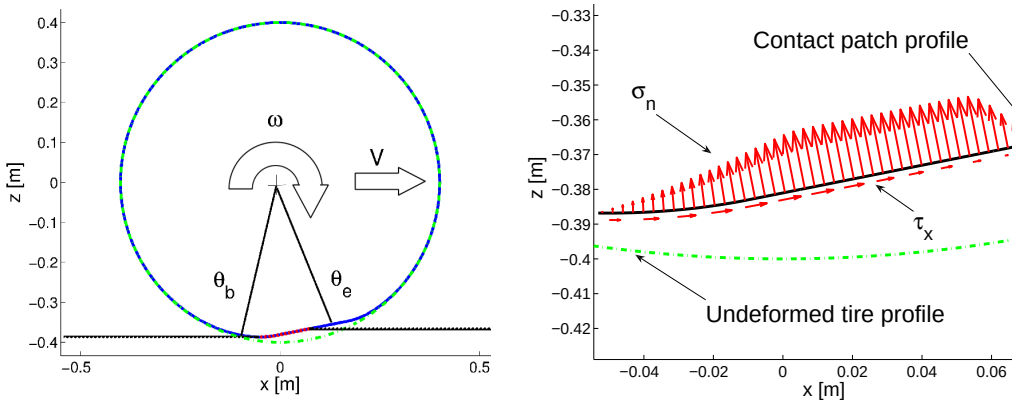

(a) (b)

Figure 1: (a) An example of a deformed tire driven on a soft surface. The tire is deforming and sinking into the ground. (b) A detail of the contact patch area. We highlight the normal stress σ_n and the tangential stress τ_x acting along the contact patch.

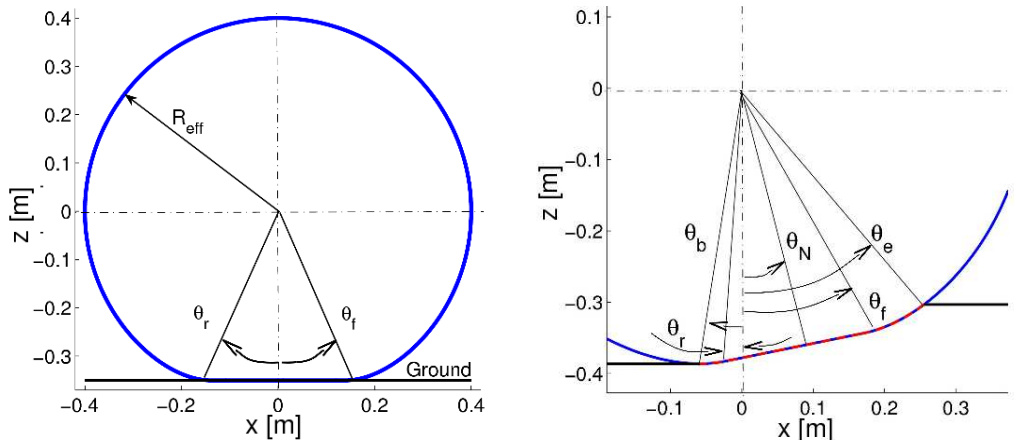

(a) (b)

Figure 2: Exaggerated plot of a deformed tire sitting on hard surface (a) and driven on a soft terrain (b). When stationary the only portion in contact with the terrain is the flat region between θ_r and θ_f which in this particular configuration correspond to θ_b and θ_e. When the tire is rolling, the section of maximum deflection is rotated on an angle $\theta_N = \frac{\theta_f}{2}$ and the entry and exit angle $\theta_{e,b}$ don't necessarily correspond to θ_f and θ_r.

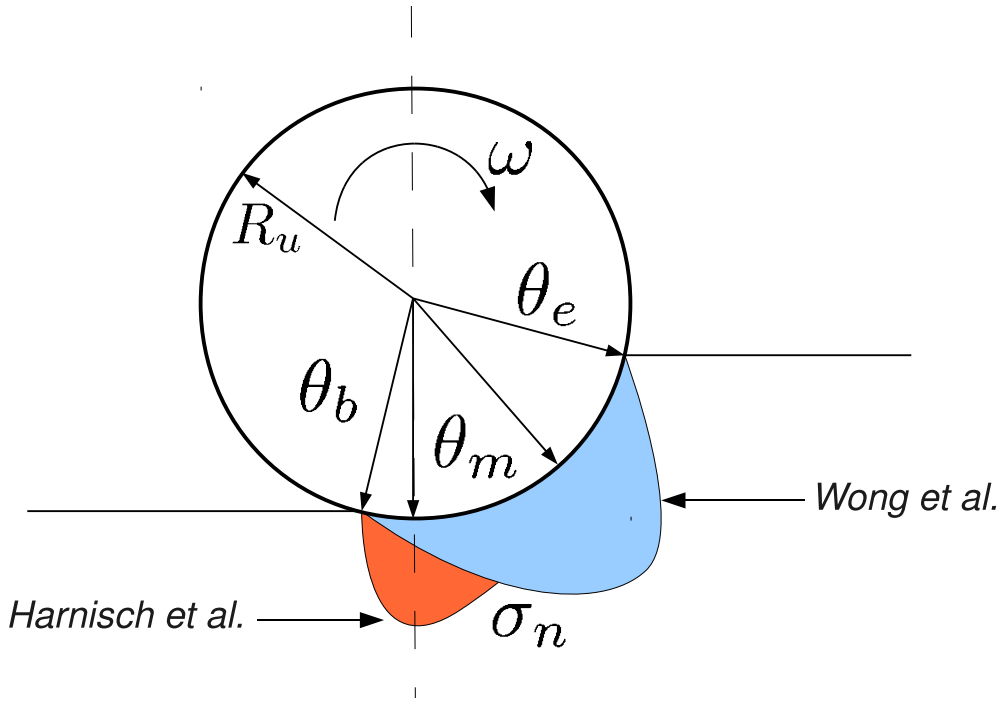

Figure 3: A schematic representation of the normal stress distribution as adopted by Harnisch et al. [12] and by Wong at al. [37]. In this paper, Wong's approach is used.

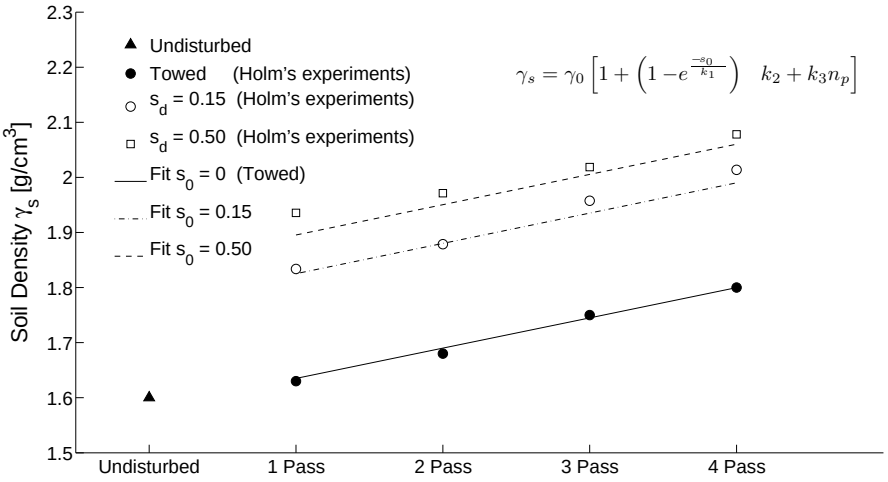

Figure 4: Variation of density recorded by Holm [14] during multipass experiments. Line fit parameters k_1, k_2 and k_3 are the same for every line.

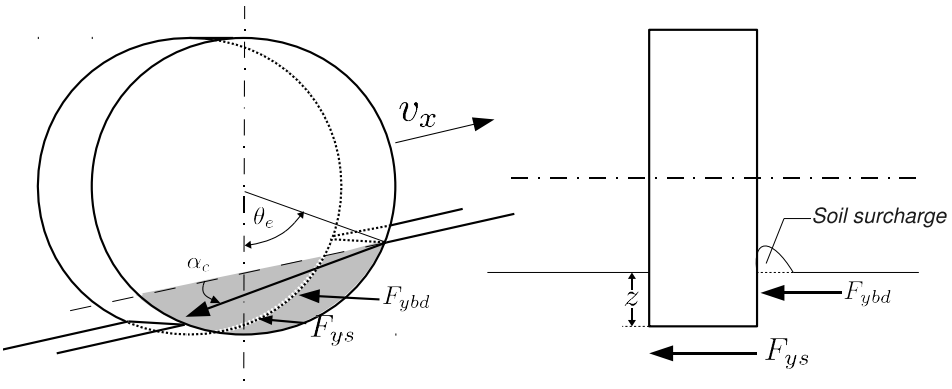

Figure 5: A schematic representation of the lateral force generation. The lateral force is composed of two components: the shear force in the lateral direction F_{ys} and the bulldozing force F_{ybd}. The first one is due to the lateral slip of the tire imposed by the steering action. This force acts on along the contact patch beneath the tire. The bulldozing force acts on the side of the tire and is due to the wheel compacting the terrain in the lateral direction.

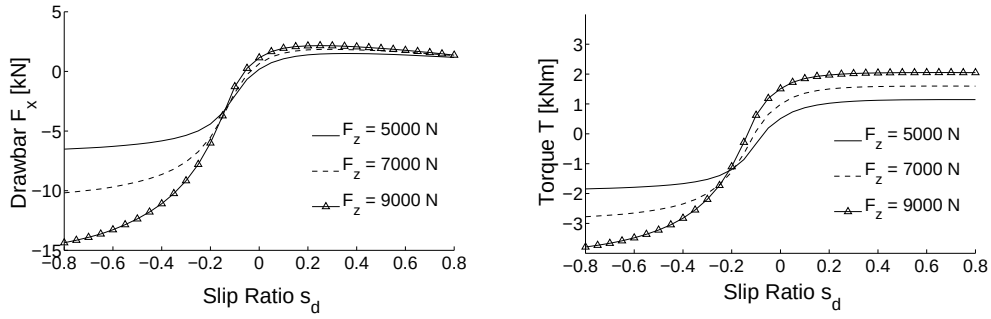

(a) (b)

Figure 6: Trend of drawbar pull and driving torque for different vertical loads and slip ratio. Dry sand, Rigid wheel.

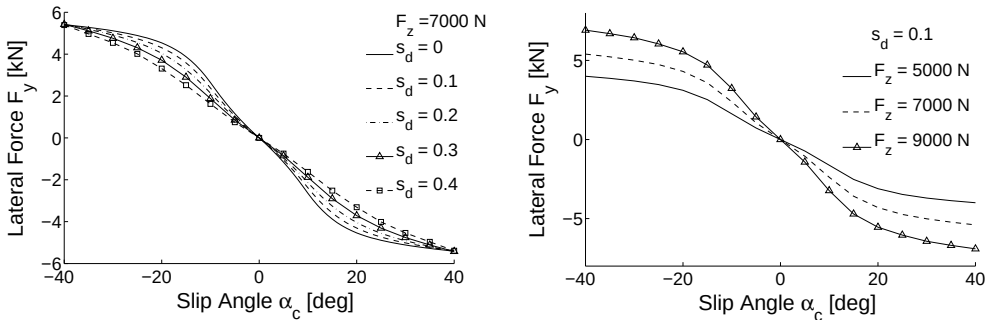

(a) (b)

Figure 7: Lateral force versus slip angle for different slip ratios and vertical loads. Dry sand, rigid wheel.

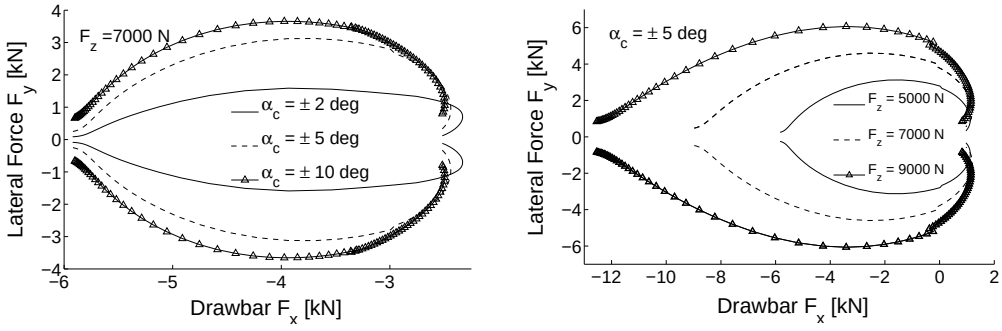

(a) (b)

Figure 8: Combined slip envelope for different slip angles and vertical loads. Dry sand, rigid wheel.

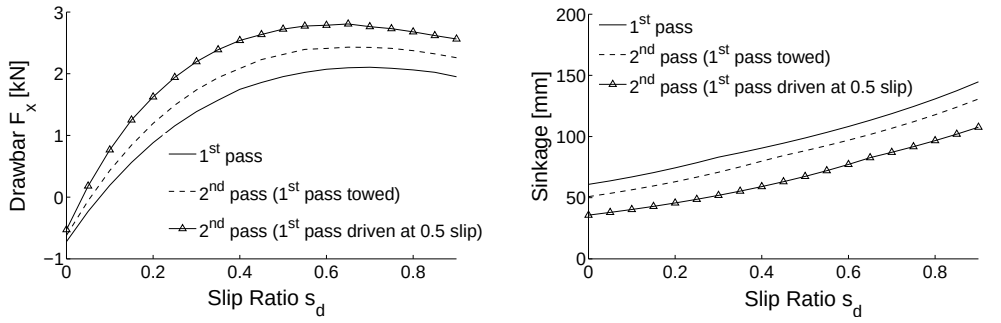

(a) (b)

Figure 9: Multi-pass influence on the performance. Dry sand, rigid wheel.

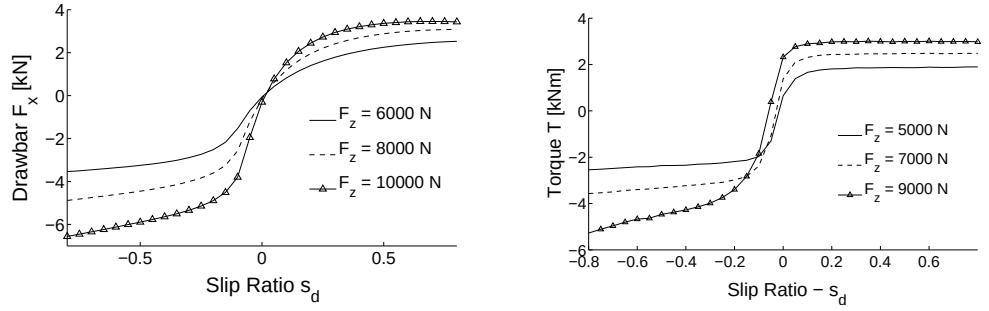

(a) (b)

Figure 10: Trend of drawbar pull and driving torque for different vertical loads and slip ratio. Moist loam, flexible tire.

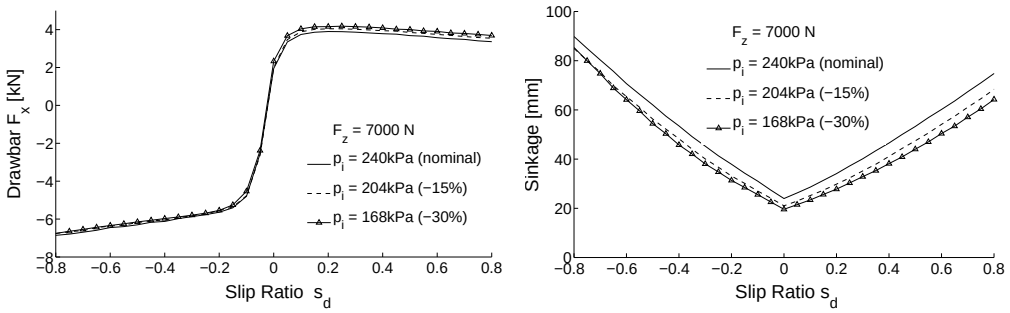

(a) (b)

Figure 11: Variation of drawbar pull with inflation pressure and trend of the sinkage with inflation pressure. Moist loam, flexible tire.

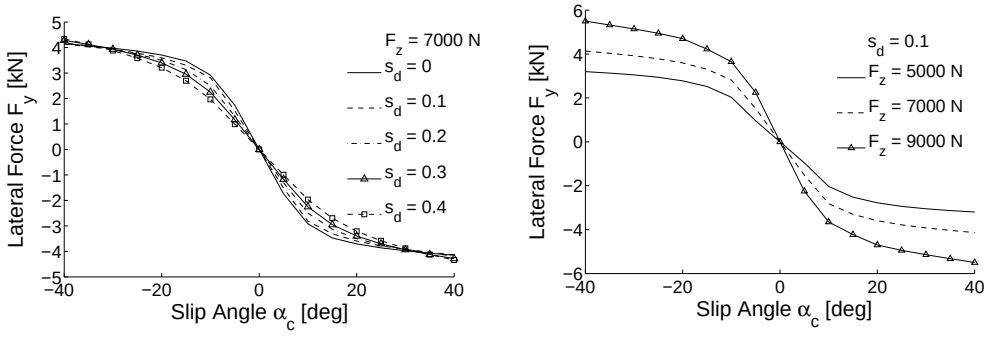

(a) (b)

Figure 12: Lateral force versus slip angle for different slip ratio and vertical load. Moist loam, flexible tire.

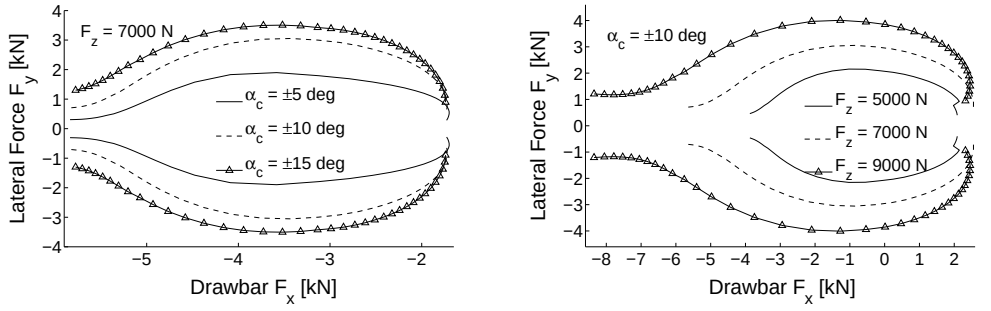

(a) (b)

Figure 13: Combined slip envelope for different slip angle and vertical load. Moist loam, flexible tire.

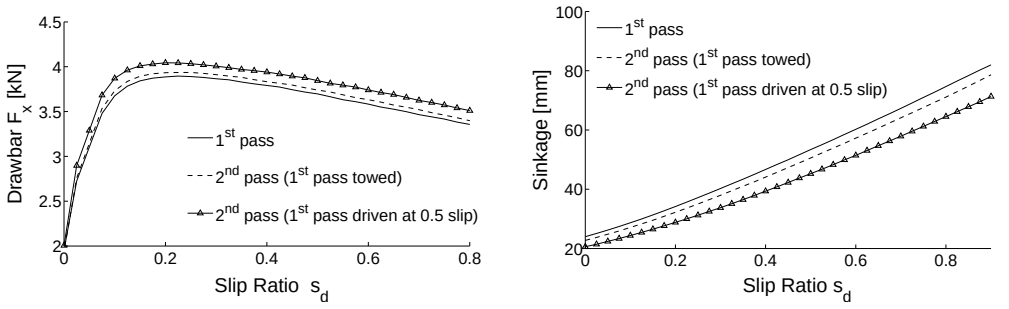

(a) (b)

Figure 14: Multi-pass influence on the performance. Moist loam, flexible tire.

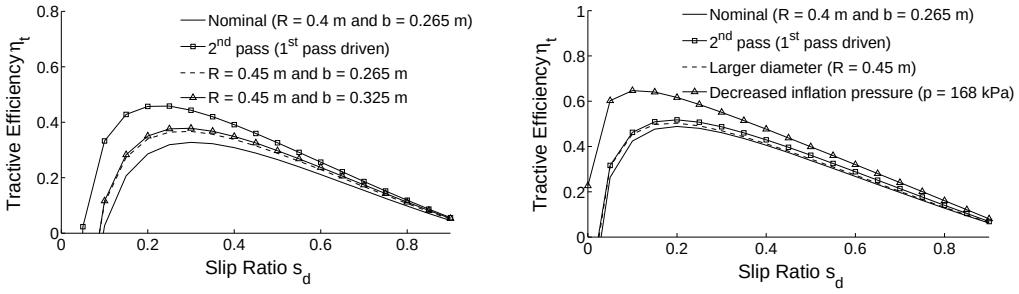

(a) (b)

Figure 15: Tractive efficiency under different operational scenarios for a tire rolling on dry sand (a) and moist loam (b).

[1] R. Bauer, W. Leung, and T. Barfoot. Experimental and simulation results of wheel-soil interaction for planetary rovers. In International Conference on Intelligent Robots and Systems, Edmonton, August 2-6 2005.

[2] M. G. Bekker. Off-The-Road Locomotion; research and development in terramechanics. The University of Michigan Press, Ann Arbor, 1960.

[3] M. G. Bekker. Introduction to Terrain-Vehicle Systems. The University of Michigan Press, Ann Arbor, 1969.

[4] W. Brixius. Traction prediction equations for bias-ply tires. In Transactions of the ASAE (871622), St. Joseph, MI, 1987.

[5] B. J. Chan. Development of an off-road capable tire model for vehicle dynamics simulations. PhD thesis, Virginia Polytechnic Institute and State University, Blacksburg, VA, 2008.

[6] B. J. Chan and C. Sandu. A novel wheel-soil interaction model for off-road vehicle dynamics simulation. In Proceedings of ASME IDETC, 9th Int. Conf. on AVTT, Sept. 4-7, Las Vegas, NV, 2007.

[7] B. J. Chan and C. Sandu. A semi-analytical approach to off-road tire modeling for vehicle dynamics simulations. In Proceedings of 16th ISTVS International Conference, Turin, Italy, 2008.

[8] B. J. Chan, N. Thompson, C. Sandu, and H. Dankowicz. A novel tire-soil interaction model for simulation of off-road vehicles. In Proceedings of 14th ISTVS International Conference, Sept. 25-29, 2005, Hayama, Japan.

[9] G. N. Durham. Powered wheels in the turned mode operating on yielding soils. Technical report, US Army Waterways Experiment Station, Vicksburg, 1976.

[10] D. R. Freitag and M. E. Smith. Center-line deflection of pneumatic tires moving in dry sand. Journal of Terramechanics, 3(1):31–46, 1966.

[11] A. Grečenko. Slip and drift of the wheel with tyre on soft ground. In Proceedings of 3rd ISTVS International Conference, volume II, pages 76–95, Essen, Germany, 1969.

[12] C. Harnisch, B. Lach, R. Jakobs, M. Troulis, and O. Nehls. A new tyre-soil interaction model for vehicle simulation on deformable ground. Vehicle System Dynamics, 43(Supplement):384–394, 2005.

[13] R. R. P. Hettiaratchi and A. R. Reece. Symmetrical three-dimensional soil failure. Journal of Terramechanics, 4(3):45–76, 1967.

[14] I. C. Holm. Multi-pass behaviour of pneumatic tires. Journal of Terramechanics, 6(3):47–71, 1969.

[15] G. Ishigami, A. Miwa, K. Nagatani, and K. Yoshida. Terramechanics-based for steering maneuver of planetary exploration rovers on loose soil. Journal of Field Robotics, 24(3):233–250, 2007.

[16] Z. Janosi and B. Hanamoto. Analytical determination of drawbar pull as a function of slip for tracked vehicles in deformable soils. In Proceedings of the 1st International Conference on Terrain-Vehicle Systems, Turin, Italy, 1961.

[17] V. V. Kacigin and V. V. Guskov. The basis of tractor performance theory. Journal of Terramechanics, 19(4):225–234, 1968.

[18] L. L. Karafiath and E. A. Nowatzki. Soil Mechanics For Off-Road Vehicle Engineering. Trans Tech Publications, Clausthal, Germany, 1978.

[19] T. Koizumi, N. Tsujiuchi, and S. Mori. Simulation of grouser-soil interaction by using 3-dimensional dem considering particle roughness. In Proceedings of 16th ISTVS International Conference, pages 221–227, Turin, Italy, 2008.

[20] C. Liang, R. W. Allen, T. J. Rosenthal, J. Chrstos, and P. Nunez. Tire modeling for off-road vehicle simulation. In Proceedings of the 2004 SAE Automotive Dynamics, Stability & Controls Conference, Detroit, MI, 2004.

[21] D. Liang, G. Hai-bo, D. Zong, and T. Jian-guo. Wheel slip-sinkage and its prediction model of lunar rover. J. Cent. South Univ. Technol., 17:129–135, 2010.

[22] H. Nakashima, H. Fujiib, A. Oidaa, M. Momozuc, Y. Kawasea, H. Kanamorid, S. Aokie, and T. Yokoyamae. Parametric analysis of lugged wheel performance for a lunar microrover by means of dem. Journal of Terramechanics, 44(2):153–162, April 2007.

[23] H. Nakashima and A. Oida. Algorithm and implementation of soiltire contact analysis code based on dynamic fede method. Journal of Terramechanics, 41:127–137, April-July 2004.

[24] S. Oida, E. Seta, H. Heguri, and K. Kato. Soil/tire interaction analysis using fem and fvm. Tire Science and Technology, 33(1):38–62, January 2005.

[25] C. Sandu, B. P. Taylor, J. S. Biggans, and M. Ahmadian. Building an infrastructure for indoor terramechanics studies: the development of a terramechanics rig at virginia tech. In Proceedings of 16th ISTVS International Conference, pages 177–185, Turin, Italy, 2008.

[26] C. Sandu, M. E. Worley, and J. P. Morgan. Experimental study on the mobility of lightweight vehicles on sand. In Proceedings of 16th ISTVS International Conference, pages 162–176, Turin, Italy, 2008.

[27] H. Schwanghart. Lateral forces on steered tyres in loose soil. Journal of Terramechanics, 1(1):9–29, 1968.

[28] H. Shibly, K. Iagnemma, and S. Dubowsky. An equivalent soil mechanics formulation for rigid wheels in deformable terrain, with application to planetary exploration rovers. Journal of Terramechanics, 42:1–13, 2005.

[29] S. Shoop, , I. Darnell, and K. Kestler. Analysis of tire models for rolling on a deformable substrate. Tire Science and Technology, 30(3):180–197, July 2002.

[30] S. Shoop, K. Kestler, and R. Haehnel. Finite element modeling of tires on snow. Tire Science and Technology, 34(1):2–37, March 2006.

[31] B. P. Taylor. Experimental evaluation and semi-empirical modeling of the tractive performance of rigid and flexible wheels on lunar soil simulant. Master's thesis, Virginia Polytechnic Institute and State University, Blacksburg, VA, 2009.

[32] K. Terzaghi, R. B. Peck, and G. Mesri. Soil Mechanics in Engineering Practice. John Wiley & Sons, New York, 3rd edition, 1996.

[33] A. Vivake, D. Delap, and C. Creager. The development of wheels for the lunar roving vehicle. Technical report, NASA, Glenn Research Center, Cleveland, OH, December 2009.

[34] J. Y. Wong. Theory Of Ground Vehicles. John Wiley & Sons, New York, 3rd edition, 2001.

[35] J. Y. Wong. Terramechanics and Off-Road Vehicle Engineering. Elsevier, UK, 2nd edition, 2010.

[36] J. Y. Wong and J. Preston-Thomas. On the characterization of the shear stress-displacement relationship of terrain. Journal of Terramechanics, 19(4):225–234, 1983.

[37] J. Y. Wong and A. R. Reece. Prediction of rigid wheel performance based on analysis of soil-wheel stresses, Part I. Performance of driven rigid wheels. Journal of Terramechanics, 4(1):81–98, 1967.

[38] J. Y. Wong and A. R. Reece. Prediction of rigid wheel performance based on analysis of soil-wheel stresses, Part II. Performance of towed rigid wheels. Journal of Terramechanics, 4(2):7–25, 1967.

[39] R. Zhang and J. Li. Simulation on mechanical behavior of cohesive soil by distinct element method. Journal of Terramechanics, 43(3):303–316, July 2006.

[40] F. M. Zoz and R. D. Grisso. Traction and tractor performance. In Agricultural Equipment Technology Conference, volume Tractor Design, Louisville, KY, February 2003.